A Compositing Approach for Preserving Significant Features in Atmospheric Profiles

RODGER A. BROWN

National Oceanic and Atmospheric Administration, Environmental Research Laboratories, National Severe Storms Laboratory, Norman, Oklahoma

28 February 1992 and 3 August 1992

ABSTRACT

Composite profiles of thermodynamic and kinematic variables are prepared to represent the characteristics of the environment within which a particular atmospheric phenomenon occurs. During the averaging process, it is desirable to retain the dominant features and associated gradients found in the individual profiles so that representative values of quantities such as flux parameters, energy budgets, convective available potential energy, and various stability indices can be computed from the composite profiles. The conventional compositing approach, where averages are computed at common heights, reduces or even smooths out a significant feature when the height and vertical extent of the feature differ from one individual profile to the next.

To retain a desirable feature in the composite profile, it is necessary to compute averages at the heights where the feature occurs and to compute the average height of the feature itself. As an example of the capabilities of this scaling or feature-preserving approach, the technique was applied to a set of 33 hodographs from supercell thunderstorm environments as documented in the literature. The feature-preserving technique retained realistic wind-shear values, including a midaltitude minimum-shear layer that disappeared when the conventional compositing technique was used.

1. Introduction

When studying a particular atmospheric phenomenon, the investigator frequently constructs a representative vertical profile of the atmosphere within which the phenomenon occurs. If a composite profile is being constructed from a large number of situations, one typically computes ensemble averages at constant heights or pressure levels. However, in doing so, one may inadvertently smooth out features in the profile that have a controlling influence on the phenomenon being studied.

For example, a common feature of the thermodynamic profile in a number of different research efforts is a subsidence inversion. Since both the height and the vertical extent of the inversion vary from one situation to the next, a composite profile based on constant pressure or height averages can decrease the sharpness found in the individual inversions to the point where the inversion may disappear. Similar problems occur at the tropopause where the height and magnitude of the coldest temperature vary from one situation to the next.

The vertical profile of the environmental wind can also be affected during the compositing process. Since the jet maximum near the tropopause varies in magnitude and height from one situation to the next, the conventional compositing process will cause the maximum to decrease in magnitude and to lose its sharpness as the peak is smeared over a larger height interval than that found in any individual profile. Within the planetary boundary layer, the wind typically veers and increases in speed with height. Since the depth of the boundary layer varies from one situation to the next, the conventional compositing process will decrease the values of vertical shear through the upper portion of the boundary layer and for some distance immediately above it.

To correct for these shortcomings, a compositing approach is described in this paper that scales individual thermodynamic and kinematic profiles so that the significant features are preserved. Of necessity, such an approach is subjective and requires the user to have a profile model in mind before it can be applied to a set of profiles. To illustrate its capability of retaining significant features, the technique is applied to 33 supercell hodographs that are documented in the meteorological literature.

2. Feature-preserving compositing approach

The purpose of a feature-preserving compositing procedure is to produce a representative profile that retains the common profile features while averaging out those features that are not consistent from profile to profile. The resulting composite profile should retain the vertical gradients as well as the values of the prominent features. One thus should be able to compute

Corresponding author address: Dr. Rodger A. Brown, National Severe Storms Laboratory, NOAA/ERL, 1313 Halley Circle, Norman, OK 73069.

Unauthenticated | Downloaded 03/01/24 11:23 PM UTC

physically realistic values for quantities such as vertical shear of the horizontal wind, energy budgets, flux parameters, convective available potential energy, bulk Richardson number, and the various stability indices.

There are a number of different ways in which profile features can be preserved. In this note, four types of features (extreme value, linear feature, nonlinear feature, and constant-slope feature) are chosen to illustrate the process. They are described as follows:

Extreme value. The value at the extreme point of the most prominent feature (such as the tropopause or jet maximum) is averaged along with its height.

Linear feature. A linear feature, such as a temperature inversion, is one where the values at the top and bottom of the feature are averaged along with their respective heights.

Nonlinear feature. If a vertical feature is not linear but has distinct lower and upper bounds, then means of values and heights are computed at the lower and upper bounds and at the same proportional distances between the bounds in each profile. If the feature has a large vertical extent, mean values at intermediate points could be computed at common heights instead.

Constant-slope feature. When a portion of a profile is fairly linear and it is bounded by features where the mean values at the bounding heights are available, only the overall slope of the linear portion needs to be averaged.

Reference height. In some situations it may be desirable to use the ground as the common reference height for the lower portions of a profile and mean sea level as the common reference height for the upper portions of a profile. The two frames of reference can be combined by computing the mean height of the ground above sea level and then subtracting that height from the feature mean heights that were computed relative to sea level or, conversely, by adding the mean height of ground above sea level to the feature mean heights that were computed relative to the ground.

An example of how this compositing approach can be applied to a temperature profile and a wind profile is shown in Fig. 1. Each profile is divided into segments, based on the characteristics of the respective profiles. For the temperature example, it is assumed that the prominent features of the set of temperature profiles are a superadiabatic layer above the surface, a nearly adiabatic layer above that, an inversion layer above the adiabatic layer, and a prominent tropopause. The temperature and height values at the bounds of each layer feature and at the tropopause are separately averaged. Then mean temperature values are computed at common heights in the nonlinear portion between the top of the inversion and the tropopause.

For the wind-component example in Fig. 1b, it is assumed that the prominent features of the set of wind profiles are an essentially uniform wind layer (nonlinear feature) at middle altitudes and a maximum value

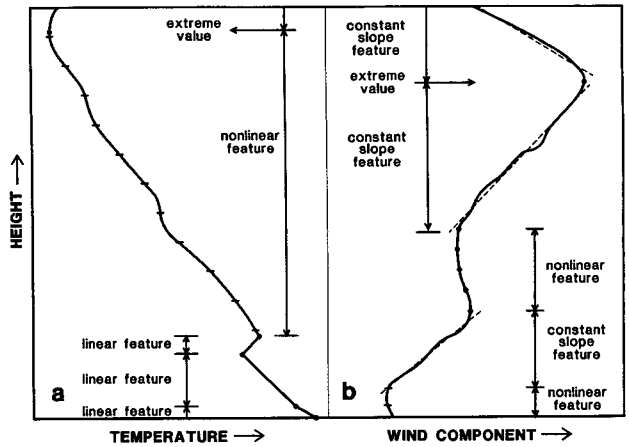

FIG. 1. Examples of vertical profiles of (a) temperature and (b) wind component with various feature-preserving elements indicated. Horizontal tick marks along curves represent constant height values, while dots represent either feature points or proportional spacing through the depth of a feature. Dashed lines represent features having a constant slope.

associated with the upper-level jet. It is also assumed that the individual profiles exhibit nearly uniform shear layers above and below the two prominent features. Near the ground, the nonlinear wind component feature is variable from profile to profile.

3. Compositing approach applied to supercell environments

To illustrate the capabilities of the feature-preserving compositing approach, it is applied to the environment within which supercell and tornadic thunderstorms form. Composite profiles representing the thermodynamic and kinematic characteristics of that environment have been prepared by a number of investigators using a variety of techniques. Profiles have been normalized by dividing them into geographical regions (e.g., Darkow 1969; Wills 1969), dividing them into storm types (e.g., Fankhauser and Mohr 1977; Bluestein and Jain 1985), or dividing them according to overall flow directions (e.g., Maddox 1976). Hodographs have been normalized by rotating them until their individual mean wind directions were oriented in the direction of the overall average mean wind (e.g., Fankhauser and Mohr 1977) or by rotating them until their associated storm-motion vectors were pointing in the same direction as the overall average storm-motion direction (e.g., Darkow and McCann 1977).

Some investigators computed averages at constant pressure levels (e.g., Fawbush and Miller 1952, 1954; Darkow 1969; Wills 1969; Maddox 1976) or at constant heights above sea level (e.g., Fankhauser and Mohr 1977; Bluestein and Jain 1985), while others computed averages at constant heights above the ground in order to maintain boundary-layer characteristics (e.g., Darkow and Fowler 1971; Darkow and

Unauthenticated | Downloaded 03/01/24 11:23 PM UTC

McCann 1977). Schaefer and Livingston (1988, 1990) normalized variations in surface height and pressure values by dividing the height interval from the surface to 100 mb into 25 logarithmically distributed levels.

Owing to the averaging procedures used in the above-cited studies, only the composite thermodynamic profiles of Fawbush and Miller (1952, 1954) showed the presence of the inversion that should have been present in most of the individual profiles. Fawbush and Miller evidently computed average temperature, humidity, and pressure at the top and bottom of the inversion, while elsewhere they computed averages at common pressure levels. None of the cited composite hodographs or vertical wind profiles showed the nearly uniform wind layer at middle altitudes found in most severe thunderstorm environments (e.g., Brown 1990).

The feature-preserving compositing approach discussed in section 2 was applied to a dataset consisting of hodographs representing the environment of supercell thunderstorms that have been documented in the literature. Since storm motion and the orientation of the hodograph vary from one storm situation to the next, the first step of the compositing process used here was to translate and rotate the ground-relative coordinate system to normalize for (a) storm motion and (b) environmental wind direction. As indicated in Fig. 2, the ground-relative coordinate origin was translated to the tip of the storm motion vector to produce a storm-relative coordinate system. Then the coordinate axes were rotated until the new u' axis was subjectively oriented parallel to the hodograph curve in the upper troposphere (that is, in the direction of the upper-tropospheric shear vector). This alignment permits the v' component (normal to, and to the left of, the u' axis) to accentuate the low-altitude, storm-relative velocity maximum associated with the low-altitude directional-shear layer. Alternatively, the u' axis could have been aligned in the direction of storm motion. For the dataset discussed below, the angle between the u' axis and the storm-motion direction was within ±30° in two-

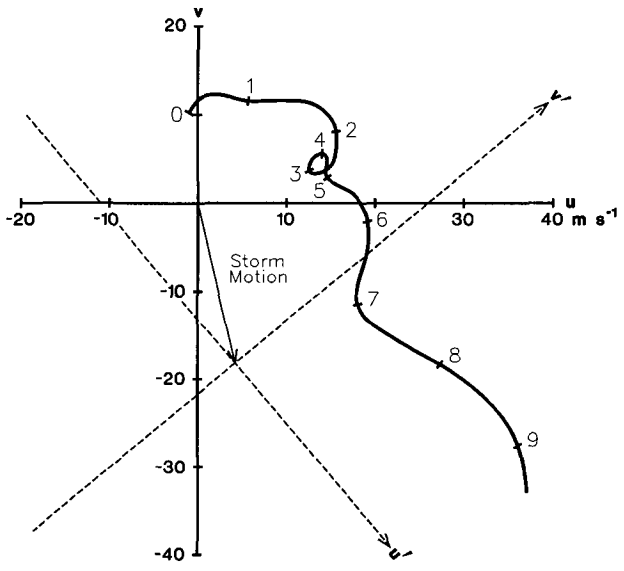

FIG. 2. Supercell hodograph (Newton 1960) plotted relative to the ground (solid coordinate axes u, v) and relative to storm motion (dashed coordinate axes u', v') with the u' axis oriented parallel to the overall upper-altitude shear vector.

TABLE 1. Hodographs of supercell environments used to produce the composite supercell hodograph.

Date	Location	Source
21 April 1958	Texas	Newton (1960, Fig. 6)
4 May 1961	Oklahoma	Browning and Donaldson (1963, Fig. 13)
3 April 1964	Oklahoma	Charba and Sasaki (1971, Fig. 12b)
27 May 1965	Oklahoma	Harrold (1966, Fig. 3)
29 June 1967	Alberta	Warner (1972, Fig. 2)
28 July 1968	Alberta	Chisholm (1973, Fig. 31)
9 August 1968	Massachusetts	Kraus (1974, Fig. 5)
25 June 1969	Oklahoma	Lemon (1976, Fig. 2)
29–30 April 1970	Oklahoma	Barnes [1978, Fig. 9 (WHT)]
18 June 1970	Colorado	Marwitz (1972, Fig. 14)
23 May 1971	Oklahoma	Brown and Crawford (1972, Fig. 1)
23 July 1971	Alberta	Renick et al. (1972, Fig. 7)
19 April 1972	Oklahoma	Brown et al. (1973, Fig. 1)
21 June 1972	Colorado	Browning and Foote (1976, Fig. 4)
24 May 1973	Oklahoma	Lemon et al. (1978, Fig. 2)
25 May 1974	Oklahoma	Nelson (1977, Fig. 1)
8 June 1974	Oklahoma	Heymsfield (1978, Fig. 3)
29 May 1976	Oklahoma	Nelson (1983, Fig. 1)
22 July 1976	Colorado	Foote and Frank (1983, Fig. 2)
1 May 1977	Oklahoma	Bluestein & Sohl (1979, Fig. 1b)
20 May 1977	Oklahoma	Ray et al. [1981, Fig. 4 (TVY)]
2 May 1979	Oklahoma	Brandes et al. (1988, Fig. 2)
19 June 1980	Oklahoma	Vasiloff et al. [1986, Fig. 5 (TTS)]
22 May 1981	Oklahoma	Davies-Jones (1984, Fig. 12)
1 August 1981	Montana	Kubesh et al. (1988, Fig. 3)
2 August 1981	Montana	Weisman et al. (1983, Fig. 2)
11 May 1982	Oklahoma	Davies-Jones (1984, Fig. 15)
26 April 1984	Oklahoma	Burgess and Curran [1985, Fig. 6 (FSI)]
13 June 1984	Colorado	Conway and Weisman (1988, Fig. 2)
22 June 1984	Illinois–Indiana	Przybylinski and Wright (1986, Fig. 1)
31 July 1987	Alberta	Bullas and Wallace (1988, Fig. 13)
28 November 1988	North Carolina	Davies-Jones et al. (1990, Fig. 1)
8 June 1989	Louisiana	Revitte (1990, Fig. 8)

Unauthenticated | Downloaded 03/01/24 11:23 PM UTC

thirds of the cases and the overall average difference was 6°.

A total of 33 hodographs for supercell environments were identified from the literature; the dates, locations, and sources of information are tabulated in Table 1. About one-half of the hodographs were from Oklahoma, one-eighth each were from Alberta and Colorado, and the remaining one-quarter were from Illinois, Indiana, Louisiana, Massachusetts, Montana, North Carolina, and Texas.

A geographical sampling of the vertical profiles of the u' and v' components is shown in Fig. 3. The u' component of the wind increased from near the ground to the height of the jet maximum (in most cases, above 10 km). The v' component had a maximum at 1–2 km above the ground and was variable at higher altitudes. The thicker portion of the v' curve represents a depth twice the height of the low-altitude peak value. The two parallel lines delineate the vertical extent of the minimum-shear layer at middle altitudes that appeared in individual hodographs as a series of overlapping loops (Fig. 3e), a single closed loop (Figs. 2, 3a, 3f, and 3g), an open loop (Figs. 3d and 3h), or as a packing of height tick marks along the hodograph curve (Figs. 3b, 3c, and 3i).

The next step of the compositing process was to tabulate the u' and v' values of the various features along with their respective heights above the ground. For this dataset, the composite profiles extended only up to the level of the jet maximum. The u' component was divided into the same segments as shown in Fig. 1b. Within the minimum-shear layer (between the two parallel lines in Fig. 3) the u' and v' curves were represented by five equally spaced points. The v' velocity peak just above the ground (thick portion of the v' curves in Fig. 3) also was represented by five equally

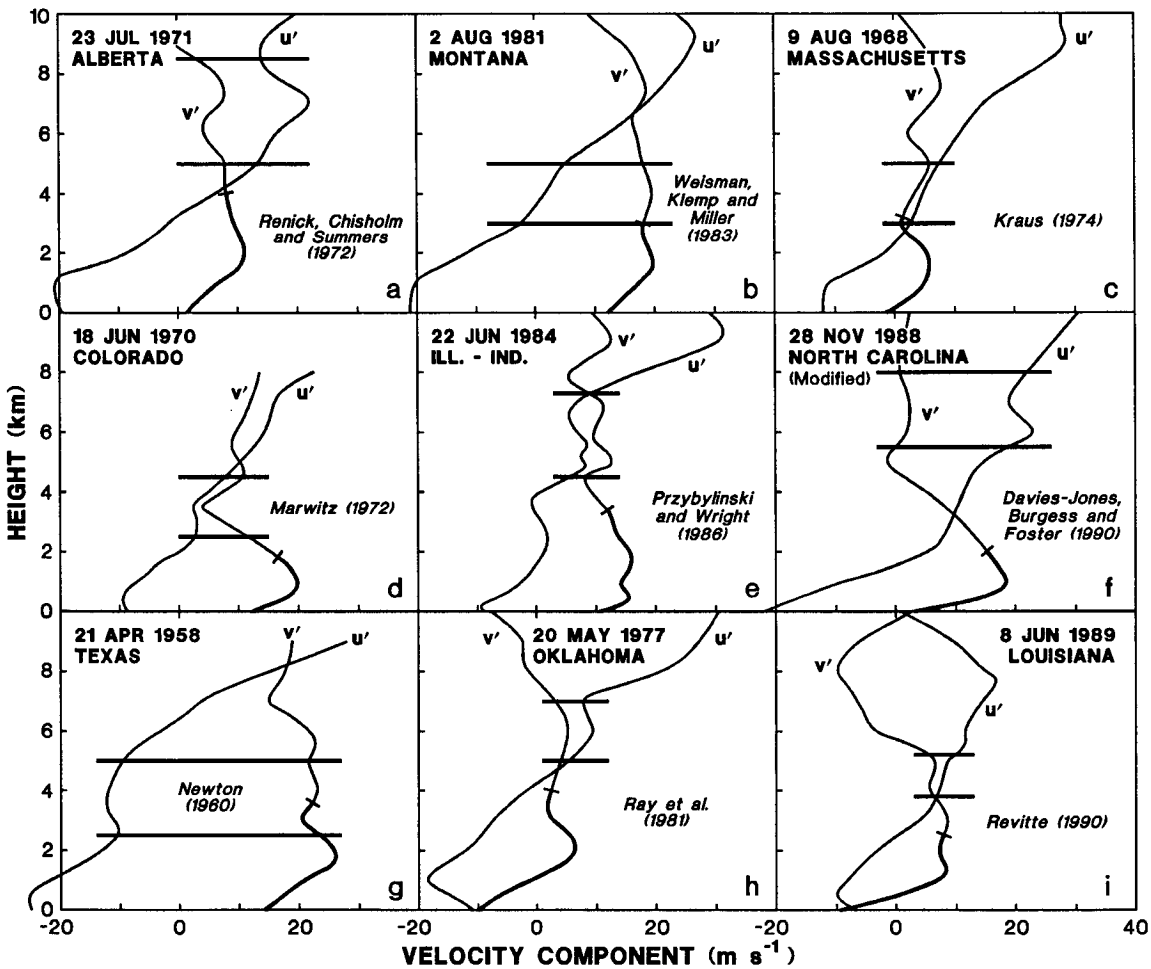

FIG. 3. Representative sample of vertical profiles of storm-relative u' and v' wind components (defined in Fig. 2) at various geographical locations across the United States and southern Canada. The thickened portion of the lower v' curves (capped by a tick mark) represents twice the depth of the storm-relative velocity maximum. The midaltitude minimum-shear layer is encompassed by the two horizontal lines.

Unauthenticated | Downloaded 03/01/24 11:23 PM UTC

spaced points that were at 0.0, 0.5, 1.0, 1.5, and 2.0 times the height of the peak value. All other portions of the v' curves were averaged at constant height levels.

After all of the values were tabulated, mean values were computed for each wind component and its associated height. Some of the features were not present in all hodographs. For example, the minimum-shear layer was not apparent in 3 of the 33 hodographs and the low-altitude v' maximum was not apparent in 3 others. Seven profiles did not extend to the height of the u' jet maximum. The peak of the v' curve occurred at a mean height of 1.3 km. The minimum-shear layer extended from 3.2 to 5.8 km, with the mean speed shear through the layer being only 0.43 m s^{-1} km^{-1}. The mean height of the u' jet maximum was 10.6 km.

For comparison purposes, both feature-averaged profiles and conventional height-averaged profiles were computed. As shown in Fig. 4, it is clear that using feature averages produces more representative profiles than does using constant-height averages. The constant-height-averaging process underestimates the peak velocity values in the low-altitude v' maximum and in the upper-altitude u' maximum, completely wipes out the midaltitude minimum-shear layer, and cuts the u' shear between 6 and 10 km nearly in half.

Standard deviations of the u' and v' values also were computed. They were between 5 and 7 m s^{-1} for u' below 6 km and for v' at all heights for both the feature-averaged profiles and height-averaged profiles. The standard deviation of u' for the height-averaged profile increased from 7 m s^{-1} at 6 km to 14 m s^{-1} at the jet maximum, 10.6 km. The larger values for u' reflect the variation of the height and u' value of the jet maximum. Based on their computations for nine supercell storms, Bluestein and Jain (1985) found that the standard deviations of both u and v (relative to north) increased from 2 m s^{-1} near the ground to 5 m s^{-1} at 2 km and to 10 m s^{-1} at 11 km.

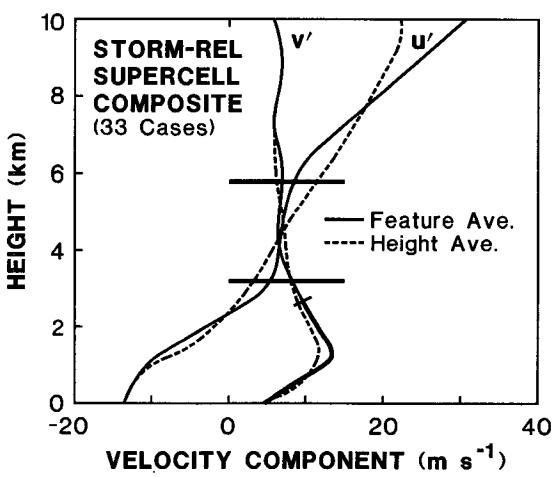

FIG. 4. Composite storm-relative profiles of u' and v' based on 33 supercell hodographs. The solid curves represent averages of common features, and the dashed curves represent averages at common heights. See Fig. 3 for additional explanations.

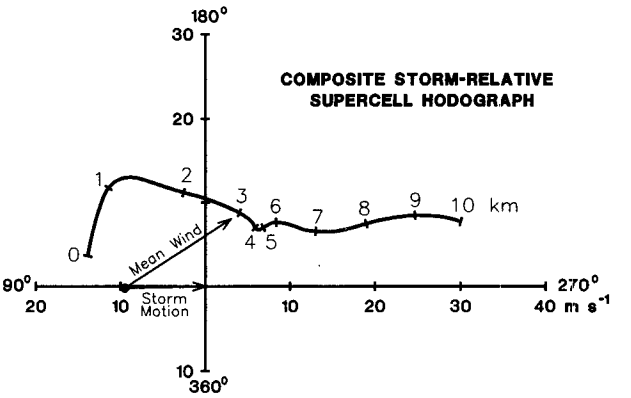

FIG. 5. Composite storm-relative hodograph for the environments within which 33 supercell thunderstorms formed, based on the feature-averaged u' and v' profiles in Fig. 4. The average storm motion and mean wind vectors emanate from the ground-relative origin.

4. Composite hodograph

The final step in the compositing process was to plot the feature-averaged u',v' hodograph and then rotate it to become relative to true north; the mean direction of the positive u' axis was 86°. The resulting composite storm-relative hodograph for the supercell environment is shown in Fig. 5. The hodograph curve clearly shows the three primary components of the supercell environment. In the directional-shear layer from the ground to 3.2 km, the wind veers about 100° from east-southeast to south-southwest. In the minimum-shear layer from 3.2 to 5.8 km, the storm-relative flow is 9–10 m s^{-1} from the south-southwest to southwest. In the speed-shear layer from 6 to 10 km, the wind increases in speed from southwesterly at 10 m s^{-1} to west-southwesterly at over 30 m s^{-1}.

In Fig. 5, the mean wind (density weighted 0–10 km computed from the composite) and the mean of the storm-motion vectors are plotted in a ground-relative framework. The mean storm motion (9.5 m s^{-1} from 269°) being from the west is a consequence of the fact that roughly the same number of storms in the sample were moving from south of west as from north of west. Storm motion was 63% of, and 32° to the right of, the mean wind (15.2 m s^{-1} from 237°); these values are close to the values of 75% and 30° used by Maddox (1976) in his study of tornado proximity soundings.

Based on theoretical considerations, Davies-Jones et al. (1990) deduced that the storm-relative hodograph that favors supercell thunderstorms (that is, those with mesocyclones) should rotate at least 90° and have storm-relative winds of at least 10 m s^{-1} in the lowest 3 km. For the composite hodograph in Fig. 5, the wind

Unauthenticated | Downloaded 03/01/24 11:23 PM UTC

direction veers 100° in the lowest 3 km and the wind speed varies between 10 and 16 m s^{-1}. Thus, the low-altitude portion of the composite hodograph exceeds the minimum theoretical specifications for a supercell hodograph.

These criteria of Davies-Jones et al. (1990) correspond to a storm-relative helicity value of 150 m^2 s^{-2}. Using proximity soundings for 28 tornado situations, they proposed that weak tornadoes (F0–F1) are associated with helicity values in the approximate range from 150 to 300 m^2 s^{-2}, that strong tornadoes (F2–F3) are associated with the approximate range from 300 to 450 m^2 s^{-2}, and that violent tornadoes (F4–F5) are associated with values greater than 450 m^2 s^{-2}. The storm-relative helicity in the lowest 3 km of the composite hodograph is about 300 m^2 s^{-2}. This value corresponds to the transition region between weak and strong tornadoes. Tornadoes were associated with 61% of the hodographs used in this study.

5. Concluding discussion

When constructing composites of vertical profiles of thermodynamic and kinematic parameters in the atmosphere, one desires to retain the prominent features that are common to most of the individual profiles. The conventional approach is to compute mean values at common heights. However, if the features that one wants to preserve are at different heights and have different vertical extents, they can be smoothed so much that they disappear in the composite profile. To prevent this undesirable situation, a compositing approach has been devised to preserve the prominent features in vertical profiles while smoothing those portions of the profiles that vary from one profile to the next.

The basic philosophy of the feature-preserving approach is to identify significant points in a set of profiles and compute averages relative to those points. Averages of both the meteorological variable and its height are computed. For the portions of a profile that exhibit no prominent or consistent features, averages at common heights may be computed. Hodographs need to be initially rotated so that they all have the same orientation; the orientation direction may be in the direction of storm motion, of the mean wind, of the mean shear, etc. Once the averages have been computed and plotted, the various segments of the composite profile need to be joined smoothly at the transition points. Whereas the conventional compositing approach is very objective, the feature-preserving approach requires human intervention to identify the prominent features and then to smooth out transitions between the various segments of the composite profiles.

To demonstrate its capabilities, the feature-preserving compositing technique was applied to a set of 33 storm-relative supercell hodograph curves obtained from the literature. Each hodograph was divided into orthogonal wind components that were parallel and perpendicular to the overall upper-altitude shear vector. Velocity components were averaged relative to the height of hodograph features rather than at constant height or pressure levels.

Using the conventional height-averaging approach, the composite hodograph for a supercell environment consists of marked directional shear in the lowest 3 km and marked speed shear from 3 to 10–12 km. Using the feature-preserving approach developed here, these two characteristics are more pronounced than they otherwise would be and a third feature becomes evident. The third feature is a nearly 3-km-deep layer at middle altitudes where the wind shear becomes a minimum (0.4 m s^{-1} km^{-1} on the average). Since the minimum-shear layer is consistently present within the environment of supercell storms and may play a physical role in the evolution of supercell storms, it should be preserved in composite wind profiles.

Acknowledgments. I appreciate the helpful comments on the manuscript provided by Dr. Thomas Matejka, Arthur Witt, and the anonymous reviewers. Joan Kimpel skillfully prepared the figures. Christina Thomas provided valuable editorial assistance with the manuscript. Melissa Hornecker assisted with the computation of the composite hodograph.

REFERENCES

Barnes, S. L., 1978: Oklahoma thunderstorms on 29–30 April 1970. Part I: Morphology of a tornadic storm. *Mon. Wea. Rev.*, **106,** 673–684.

Bluestein, H. B., and M. H. Jain, 1985: Formation of mesoscale lines of precipitation: Severe squall lines in Oklahoma during the spring. *J. Atmos. Sci.*, **42,** 1711–1732.

——, and C. J. Sohl, 1979: Some observations of a splitting severe thunderstorm. *Mon. Wea. Rev.*, **107,** 861–878.

Brandes, E. A., R. P. Davies-Jones, and B. C. Johnson, 1988: Streamwise vorticity effects on supercell morphology and persistence. *J. Atmos. Sci.*, **45,** 947–963.

Brown, R. A., 1990: Characteristics of supercell hodographs. Preprints, *16th Conf. on Severe Local Storms,* Kananaskis Park, Alberta, Amer. Meteor. Soc., 30–33.

——, and K. C. Crawford, 1972: Doppler radar evidence of severe storm high-reflectivity cores acting as obstacles to airflow. Preprints, *15th Radar Meteor. Conf.,* Champaign–Urbana, IL, Amer. Meteor. Soc., 16–21.

——, D. W. Burgess, and K. C. Crawford, 1973: Twin tornado cyclones within a severe thunderstorm: Single Doppler radar observations. *Weatherwise,* **26,** 63–69, 71.

Browning, K. A., and R. J. Donaldson, Jr., 1963: Airflow and structure of a tornadic storm. *J. Atmos. Sci.*, **20,** 533–545.

——, and G. B. Foote, 1976: Airflow and hail growth in supercell storms and some implications for hail suppression. *Quart. J. Roy. Meteor. Soc.*, **102,** 499–533.

Bullas, J. M., and A. F. Wallace, 1988: The Edmonton tornado, July 31, 1987. Preprints, *15th Conf. on Severe Local Storms,* Baltimore, MD, Amer. Meteor. Soc., 437–443.

Burgess, D. W., and E. B. Curran, 1985: The relationship of storm type to environment in Oklahoma on 26 April 1984. Preprints, *14th Conf. on Severe Local Storms,* Indianapolis, IN, Amer. Meteor. Soc., 208–211.

Unauthenticated | Downloaded 03/01/24 11:23 PM UTC

Charba, J., and Y. Sasaki, 1971: Structure and movement of the severe thunderstorms of 3 April 1964 as revealed from radar and surface mesonetwork data analysis. *J. Meteor. Soc. Japan,* **49,** 191–214.

Chisholm, A. J., 1973: *Alberta hailstorms. Part I: Radar case studies and airflow models. Meteor. Monogr.,* No. 14, Amer. Meteor. Soc., 1–36.

Conway, J. W., and M. L. Weisman, 1988: An investigation into the splitting and propagation of the 13 June 1984 Denver hailstorms. Preprints, *15th Conf. on Severe Local Storms,* Baltimore, Amer. Meteor. Soc., 276–279.

Darkow, G. L., 1969: An analysis of over sixty tornado proximity soundings. Preprints, *Sixth Conf. on Severe Local Storms,* Chicago, Amer. Meteor. Soc., 218–221.

——, and M. G. Fowler, 1971: Tornado proximity sounding wind analysis. Preprints, *Seventh Conf. on Severe Local Storms,* Kansas City, Amer. Meteor. Soc., 148–151.

——, and D. W. McCann, 1977: Relative environmental winds for 121 tornado bearing storms. Preprints, *Tenth Conf. on Severe Local Storms,* Omaha, Amer. Meteor. Soc., 413–417.

Davies-Jones, R. P., 1984: Streamwise vorticity: The origin of updraft rotation in supercell storms. *J. Atmos. Sci.,* **41,** 2991–3006.

——, D. Burgess, and M. Foster, 1990: Test of helicity as a tornado forecast parameter. Preprints, *16th Conf. on Severe Local Storms,* Kananaskis Park, Alberta, Amer. Meteor. Soc., 588–592.

Fankhauser, J. C., and C. G. Mohr, 1977: Some correlations between various sounding parameters and hailstorm characteristics in northeast Colorado. Preprints, *Tenth Conf. on Severe Local Storms,* Omaha, Amer. Meteor. Soc., 218–225.

Fawbush, E. J., and R. C. Miller, 1952: A mean sounding representative of the tornadic airmass environment. *Bull. Amer. Meteor. Soc.,* **33,** 303–307.

——, and ——, 1954: The types of airmasses in which North American tornadoes form. *Bull. Amer. Meteor. Soc.,* **35,** 154–165.

Foote, G. B., and H. W. Frank, 1983: Case study of a hailstorm in Colorado. Part III: Airflow from triple-Doppler measurements. *J. Atmos. Sci.,* **40,** 686–707.

Harrold, T. W., 1966: A note on the development and movement of storms over Oklahoma on May 27, 1965. ESSA Tech. Memo. IERTM-NSSL-29, National Severe Storms Laboratory, 1–8. [NTIS, AD-644899.]

Heymsfield, G. M., 1978: Kinematic and dynamic aspects of the Harrah tornadic storm analyzed from dual-Doppler data. *Mon. Wea. Rev.,* **106,** 233–254.

Kraus, M. J., 1974: Doppler radar investigation of flow patterns within thunderstorms. Environ. Res. Papers No. 481, AFCRL-TR-74-0290, Air Force Cambridge Research Laboratories, 86 pp. [NTIS, ADA002371.]

Kubesh, R. J., D. J. Musil, R. D. Farley, and H. D. Orville, 1988: The 1 August 1981 CCOPE storm: Observations and modeling results. *J. Appl. Meteor.,* **27,** 216–243.

Lemon, L. R., 1976: The flanking line, a severe thunderstorm intensification source. *J. Atmos. Sci.,* **33,** 686–694.

——, D. W. Burgess, and R. A. Brown, 1978: Tornadic storm airflow and morphology derived from single-Doppler radar measurements. *Mon. Wea. Rev.,* **106,** 48–61.

Maddox, R. A., 1976: An evaluation of tornado proximity wind and stability data. *Mon. Wea. Rev.,* **104,** 133–142.

Marwitz, J. D., 1972: The structure and motion of severe hailstorms. Part I: Supercell storms. *J. Appl. Meteor.,* **11,** 166–179.

Nelson, S. P., 1977: Rear flank downdraft: A hailstorm intensification mechanism. Preprints, *Tenth Conf. on Severe Local Storms,* Omaha, Amer. Meteor. Soc., 521–525.

——, 1983: The influence of storm flow structure on hail growth. *J. Atmos. Sci.,* **40,** 1965–1983.

Newton, C. W., 1960: Morphology of thunderstorms and hailstorms as affected by vertical wind shear. *Physics of Precipitation,* H. Weickmann, Ed., American Geophysical Union, 339–347.

Przybylinski, R. W., and J. E. Wright, Jr., 1986: Analysis of severe convection and merging storms on 22 June 1984 with conventional and Doppler radar. *Natl. Wea. Dig.,* **11**(3), 6–17.

Ray, P. S., B. C. Johnson, K. W. Johnson, J. S. Bradberry, J. J. Stephens, K. K. Wagner, R. B. Wilhelmson, and J. B. Klemp, 1981: The morphology of several tornadic storms on 20 May 1977. *J. Atmos. Sci.,* **38,** 1643–1663.

Renick, J. H., A. J. Chisholm, and P. W. Summers, 1972: The seedability of multicell and supercell hailstorms using droppable pyrotechnic flares. Alberta Hail Studies 1972, Hail Studies Report 72-2, Research Council of Alberta, Edmonton, 40–46. [Available from the Research Council of Alberta, Edmonton, Alberta, Canada.]

Revitte, F. J., 1990: Description and analysis of a series of tornado occurrences in southeast Louisiana on June 8, 1989. Preprints, *16th Conf. on Severe Local Storms,* Amer. Meteor. Soc., 510–515.

Schaefer, J. T., and R. L. Livingston, 1988: The typical structure of tornado proximity soundings. *J. Geophys. Res.,* **93,** 5351–5364.

——, and ——, 1990: The evolution of tornado proximity soundings. Preprints, *16th Conf. on Severe Local Storms,* Kananaskis Park, Alberta, Amer. Meteor. Soc., 96–101.

Vasiloff, S. V., E. A. Brandes, R. P. Davies-Jones, and P. S. Ray, 1986: An investigation of the transition from multicell to supercell storms. *J. Climate Appl. Meteor.,* **25,** 1022–1036.

Warner, C., 1972: Calculations of updraft shapes in storms. *J. Atmos. Sci.,* **29,** 1516–1519.

Weisman, M. L., J. B. Klemp, and L. J. Miller, 1983: Modeling and Doppler analysis of the CCOPE August 2 supercell storm. Preprints, *13th Conf. on Severe Local Storms,* Tulsa, Amer. Meteor. Soc., 223–226.

Wills, T. G., 1969: Characteristics of the tornado environment as deduced from proximity soundings. Preprints, *Sixth Conf. on Severe Local Storms,* Chicago, Amer. Meteor. ,Soc. 222–229.

Unauthenticated | Downloaded 03/01/24 11:23 PM UTC